A systems theoretic approach to analysis and control of mammalian circadian dynamics

John H. Abel[a], Francis J. Doyle III[b]

[a]*Department of Systems Biology, Harvard Medical School, Boston, MA 02115*
[b]*Harvard John A. Paulson School of Engineering and Applied Sciences, Harvard University, Cambridge, MA 02138*

Abstract

The mammalian circadian clock is a complex multi-scale, multivariable biological control system. In the past two decades, methods from systems engineering have led to numerous insights into the architecture and functionality of this system. In this review, we examine the mammalian circadian system through a process systems lens. We present a mathematical framework for examining the cellular circadian oscillator, and show recent extensions for understanding population-scale dynamics. We provide an overview of the routes by which the circadian system can be systemically manipulated, and present *in silico* proof of concept results for phase resetting of the clock via model predictive control.

Keywords: Systems biology, process control, nonlinear dynamics, circadian rhythm, biomedical control

1. Introduction

Circadian rhythms are endogenous oscillations in gene expression, metabolism, and behavior that allow an organism to adjust its internal state to predictable cyclic changes in the environment. This advantageous feed-forward approach allows an organism with a circadian rhythm to anticipate cyclic environmental variability and adjust its physiology without a time lag. Circadian regulation of biological processes is therefore highly-conserved: these rhythms have been identified in diverse species from mammals, insects, plants, and fungi to prokaryotic cyanobacteria [1–4]. Although circadian clocks share common properties between species, the mechanistic origins and complexity of these rhythms can vary significantly. Prokaryotes have been shown to use minimal phosphorylation-based nontranscriptional oscillators, which may be reconstituted *in vitro* [5, 6]. Meanwhile, eukaryotic organisms employ transcriptional-translational feedback loops in addition to post-translational protein modification for timekeeping [7, 8]. In larger organisms such as mammals, circadian rhythms must be coordinated across cells and tissues, resulting in a complex yet robust circadian control system [9, 10].

The inherently complex nature of these processes has necessitated mathematical modeling and systems approaches for understanding biological clocks. These approaches include mechanistic and empirical process modeling [11–19], robustness and sensitivity analysis [13, 20–25], and optimal control [10, 26–29]. This review highlights the role of systems engineering in developing an understanding of, and artificially exerting control over, the mammalian circadian system.

1.1. Properties of the circadian clock

Circadian rhythms are distinguished from other periodic biological processes by several criteria [30]. First, circadian rhythms are endogenous, that is, they are self-sustained even in constant environmental conditions. Second, circadian clocks are entrainable and shift in phase or period to align with environmental cycles through cues referred to as *zeitgebers*[1]. Third, they are temperature-compensated, meaning oscillator period is insensitive to changes in temperature in the external environment. Finally, circadian rhythms have oscillatory periods of approximately, though often not exactly, 24 hours. Counter-intuitively, a near-24h period may be more advantageous than an exactly-24h period, as it provides increased stability of entrained phase angle [30].

In mammals, circadian rhythms are generated within individual cells by a network of interlocked genetic feedback loops [7, 31, 32]. These cell-autonomous clocks are responsible for regulation of genetic expression and metabolic processes in local tissue. For example, circadian regulation of glucose metabolism is localized to liver tissue, and the deletion of core clock genes in only liver tissue is sufficient to abolish circadian rhythms in expression of glucose regulatory genes [33]. This view is supported by studies demonstrating that rhythmic gene expression profiles are tissue-specific [34, 35]. Cellular rhythms are coordinated across tissues in the body and entrained to environmental rhythms through signals from the brain. The hypothalamic suprachiasmatic nucleus (SCN) is considered the "master clock" in mammals: it is responsible for entraining to light inputs and maintaining synchrony among the cell-autonomous oscillators in peripheral tissues throughout the body [9]. Peripheral tissues receive local inputs in addition to SCN signals, for example, cells in the liver may be entrained by rhythmic feeding independently of the SCN [36]. Finally, it is thought that peripheral clocks exert a degree of feedback into the SCN, though whether this is direct or indirect remains unknown [37].

[1]Trans. German: Time-givers

1.2. A need for understanding and control of the clock

It is estimated that approximately 10% of all mammalian transcripts are under circadian regulation [38]. With such widespread influence, it is unsurprising that circadian rhythms play an important role in human health and disease. In particular, high amplitudes of circadian transcription factors in peripheral tissues are desirable for good metabolic health. Mice lacking circadian rhythms due to core clock gene knockouts, or with diminished circadian amplitude due to diet or age have been shown to develop diseases, including metabolic syndrome and diabetes [39–41]. Similarly, lifestyle factors such as shift work can cause misaligned circadian cues, resulting in diminished amplitude of circadian oscillation, and ultimately, adverse health outcomes [37, 42, 43]. Neurological diseases such as posttraumatic stress disorder (PTSD), depression, and addiction are also associated with circadian disregulation [44–46]. Thus, a general aim of the study of the circadian clock is the development of pharmacological or behavioral therapies for maintaining high-amplitude circadian rhythms, or easing the effects of circadian phase resetting during jet-lag or shift work. Relatedly, there is interest in how circadian rhythms affect drug metabolism and efficacy, especially with respect to cancer medication due to circadian control of cell cycles [47, 48]. To develop such therapies, the mammalian circadian clock must be investigated mechanistically as a dynamical system.

2. The mammalian circadian control system

Circadian rhythms in mammals are generated within individual cells by interlocked transcriptional-translational feedback loops [31]. The cell-autonomous genetic clock is largely conserved across cell types, with the notable exception of red blood cells, which lack a nucleus and may compensate with a non-transcriptional clock [49]. Although the core clock is conserved, the genes under clock control may vary with cell type, creating a temporal architecture of gene expression across the body.

2.1. The cell-autonomous circadian clock

A schematic of the core clock is shown in Fig. 1A. The interlocked positive (dotted lines) and negative feedback loops (solid lines) are considered the primary source of circadian oscillation [31, 32]. Within the negative loop, isoforms of the *Period* (*Per1,2,3*) and *Cryptochrome* (*Cry1,2*) are transcribed and translated, and form heterodimers. PER-CRY heterodimers reenter the nucleus, and repress transcription of Enhancer box (E box) genes including *Per* and *Cry* through sequestration of E box activator CLOCK-BMAL1 by dissociated CRY [50]. Over time, nuclear PER and CRY is degraded, allowing transcription to resume. This negative loop is balanced by an interlocked positive feedback loop regulating the expression of *Bmal1*. In this loop, E box-controlled genes *Rev-erbα* and *Rorα* repress and promote *Bmal1* transcription, respectively, through competitive binding to the ROR/REV-ERB Response Element (RRE) in the *Bmal1* promoter [51]. Collectively, the genes *Per*, *Cry*, *Clock*, and *Bmal1* are considered the core circadian clock.

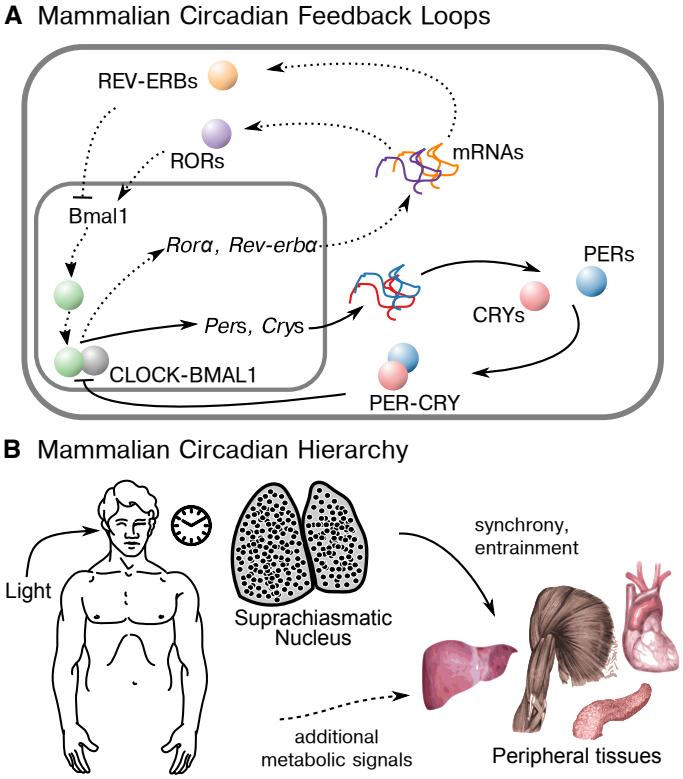

Figure 1: Schematic of the mammalian cell-autonomous clock and circadian system hierarchy. (**A**) Two interlocked feedback loops comprise the mammalian circadian oscillator: the PER-CRY negative feedback loop (solid lines), and the CLOCK-BMAL1 positive feedback loop (dotted lines). Diagram adapted from [31]. (**B**) The suprachiasmatic nucleus of the brain is the mammalian "master clock," responsible for entrainment to external light cycles and synchronizing peripheral oscillators such as those within the liver, muscle, heart, and pancreas. Within the SCN, neurons exchange neuropeptidergic and electrical signals to maintain synchrony.

The core clock regulates cellular transcription of clock-controlled genes (CCGs) via RREs, E boxes, and D boxes (DBP binding elements) [52]. Because the transcription factors corresponding to these elements peak at different circadian times, transcription of genes may be partitioned into various times of day. The core clock is also affected by a wide variety of cell type-specific transcription factors or posttranslational regulators. A genome-wide RNAi screen identified hundreds of genes with phenotypic effects on clock period or amplitude, indicating that clock pathways are highly interconnected with other, often tissue-specific metabolic pathways [53].

2.2. Stochasticity in the clock

Macroscale chemical processes may be approximated with continuous chemical kinetics, however, the low copy number of genes, transcripts, and proteins within an individual cell results in considerable deviation from continuous kinetics [55]. Stochasticity, or molecular noise, caused by the discrete nature of biochemical reactions, is referred to as *intrinsic* stochasticity. Although circadian rhythms are precise at the organism-scale, there is a significant degree of intrinsic stochasticity in

Table 1: A non-exhaustive list of notable mammalian circadian models demonstrating the range in scale and scope of such models. While not specific to circadian oscillation, the structure of the Goodwin oscillator is a common framework for circadian analysis.

Reference	Dynamic States	Kinetic Parameters	Model Form
Goodwin 1965 [54]	3	6	generalized mechanistic ODE oscillator
Kronauer *et al.* 1999 [11]	3	9	empirical ODE oscillator with human light response dynamics
Leloup and Goldbeter 2003 [13]	16	53	mammalian mechanistic ODE model
Forger and Peskin 2005 [15]	73	36	mammalian mechanistic, stochastic CME model
To *et al.* 2007 [16]	17	62	multicellular mammalian mechanistic ODE model

circadian oscillation at the single-cell scale. The cycle-to-cycle variation in circadian period within a single cell is due to intrinsic stochasticity [56]. Intrinsic stochasticity may be captured computationally through the use of stochastic simulation algorithms [15, 20]. Cellular reactions are also subject to *extrinsic* stochasticity, caused by differences between cells or within the microscopic environment, including gradients in temperature, or differences in cell cycle phase, cell size, or organelle distribution. Extrinsic stochasticity may be simulated by introducing a variability in model parametrization. Intrinsic and extrinsic variability have been studied in the circadian clock experimentally [56, 57] and computationally [15, 18, 20, 21, 58–60]. Within the circadian system, communication between cells and tissues allows the maintenance of a precise circadian phase, and adaptation to environmental cues.

2.3. Hierarchy of clocks in the body

Mammalian circadian hierarchy, shown in Fig. 1B, enables the coordination of circadian oscillation through the organism. The suprachiasmatic nucleus (SCN), the "master clock," consists of approximately 20,000 neurons within the hypothalamus. Neurons within the SCN synchronize spontaneously and therefore maintain tissue-scale oscillation indefinitely *in vitro*, whereas other tissues which lack intercellular communication display a damped oscillation likely due to gradual dephasing [57, 61]. SCN neurons exchange neuropeptidergic and electrical signals to synchronize [9]. Of primary importance are the neuropeptides vasoactive intestinal peptide (VIP) and γ-aminobutyric acid (GABA) [62–65]. The SCN is commonly divided into two regions: a ventral "core" and a dorsal "shell," which differ in neuropeptide expression and response, and neuronal network structure [9, 64–68]. The SCN entrains through its core region receiving light input from the retinohypothalamic tract (RHT) [9]. The SCN then adjusts its phase of oscillation to match light cues, and the shell region outputs time of day cues to connected brain regions and ultimately the rest of the body [69].

Peripheral tissues sustain oscillation in the absence of a functional SCN, however, signals from the SCN are necessary to maintain a coherent phase [9]. These signals from the SCN include sympathetic and parasympathetic pathways, hormonal rhythms, and temperature [32]. In addition to signals from the SCN, peripheral tissues receive local metabolic cues which help to establish circadian phase. Glucose, glucocorticoids, insulin, and other common metabolic factors have been shown to influence the clock, and it is possible that multiple metabolic signals are simultaneously responsible for modulating peripheral clocks [37, 70]. Restricted feeding in rodents has been shown to effectively decouple liver cells from the SCN and shift circadian phase by nearly 180°, indicating that metabolic cues form an important component of the circadian system [71].

3. Quantitative analysis of circadian dynamics

In the past several decades, significant advances in understanding circadian rhythms have been made through the use of mathematical modeling. Here, we present an introduction to sensitivity analysis and modeling of the circadian clock, with a focus on ordinary differential equation models. Section 3.1 introduces the concept of a limit cycle oscillator, a dynamical system commonly used to describe circadian clockwork. Section 3.2 introduces a variety of quantitative tools for the analysis of a single limit cycle oscillator, and 3.3 expands upon these tools for the analysis of a population of oscillators. Sections 3.4 and 3.5 provide derivations of the tools introduced in 3.2 and 3.3, respectively, and comment on how these quantities may be calculated. For the casual reader, 3.4 and 3.5 may be omitted without loss of qualitative understanding.

Circadian clock dynamics are commonly modeled through coupled nonlinear equations. Broadly, clock models may be empirical (i.e., designed to capture clock behavior without regard for the underlying physical system), or mechanistic (i.e., comprised of the underlying species and their mathematical relationships). Furthermore, these models may consist of deterministic ordinary differential equations (ODEs) [11–13, 16, 17, 19, 72], a discrete stochastic chemical master equation (CME) [15, 18, 20, 59], or Langevin stochastic differential equations (SDEs) [73, 74]. Stochastic approaches are generally utilized in cases where intrinsic molecular noise is thought to be significant. A description and the dimensions of five notable circadian models are provided in Table 1.

Irrespective of these possibilities, the circadian clock is primarily modeled as a deterministic set of ODEs comprising a limit cycle oscillator. This is because the circadian oscillator exhibits limit cycle-like behavior: it has a self-sustained oscillation with stable waveform and amplitude, the oscillator manifold is attractive, and perturbations to oscillation result in a phase shift. The dynamics of a limit cycle oscillator are additionally useful for explaining entrainment and phase and amplitude response behavior of the circadian oscillator.

3.1. The limit cycle oscillator

Limit cycle oscillators are not unique to biology, for example, they have been utilized to describe oscillatory chemical reactions [75], electrical circuits [76], and earthquakes [77]. As such, some of the following tools were first conceptualized outside of the context of biological rhythms. For this work, we are exclusively interested in tools developed to describe attractive limit cycles. An attractive limit cycle oscillator consists of a set of coupled ODEs of the form:

$$\frac{d\mathbf{x}}{dt} = \mathbf{f}(\mathbf{x}(t), \mathbf{p}), \tag{1}$$

which satisfies:

$$\lim_{t\to\infty}[\mathbf{x}(t) - \mathbf{x}(t-\tau)] = 0. \tag{2}$$

The steady state limit cycle is therefore the closed oscillatory path $\mathbf{x}^\gamma$ which is traversed with a period of τ, where τ is the smallest positive value for which Eq. 2 holds. For mechanistic models, $\mathbf{x} \in \mathbb{R}^n$ is a vector of state concentrations, $\mathbf{p} \in \mathbb{R}^m$ are kinetic parameters, and $\frac{d\mathbf{x}}{dt} = \mathbf{f}(\mathbf{x}(t), \mathbf{p})$ are differential material balance equations, of the form:

$$\frac{dx}{dt} = r_{x,in} - r_{x,out} + r_{x,generation} - r_{x,consumption} \tag{3}$$

for each of n species. The rate terms comprising the right hand side of Eq. 3 may follow mass-action, Michaelis-Menten, or Hill kinetics, providing an explicit mathematical analogy with the treatment of a continuous stirred tank reactor (CSTR) system. Here, the concentrations of mRNA and protein species correspond with the reactants and products in a CSTR, and the volume of the subcellular compartment in which each species resides corresponds to CSTR volume. However, concentrations are often provided in arbitrary concentration units for simplicity without loss of information. Empirical models need not conform to this physicality, and as such the Van der Pol oscillator is commonly used [11]. For simplicity, we will continue with our treatment of a mechanistic model, though the same tools apply to empirical models differing only in interpretation.

Each unique point on the stable limit cycle $\mathbf{x}^\gamma$ corresponds to a unique phase $\phi \in [0, \tau)$. Following the definition in [10, 22], we refer to the *phase* as the time distance from a reference point $\mathbf{x}_0^\gamma$ on the limit cycle, modulo the period. Intuitively, phase increases linearly with respect to time along the path $\mathbf{x}^\gamma$:

$$\frac{d\phi(\mathbf{x}^\gamma(t), \mathbf{p})}{dt} = 1, \quad \phi(\mathbf{x}_0^\gamma) = 0. \tag{4}$$

For convenience, the limit cycle oscillator described in Eqs. 1 and 2 may be rescaled to have $\tau = 2\pi$ without loss of dynamics, constraining the phase $\phi \in [0, 2\pi)$ and allowing the direct application of circular statistics [78]:

$$\tilde{t} = \frac{2\pi}{\tau}t, \quad \tilde{f} = \frac{\tau}{2\pi}f, \quad \frac{d\mathbf{x}}{d\tilde{t}} = \tilde{\mathbf{f}}(\mathbf{x}(\tilde{t}), \mathbf{p}). \tag{5}$$

3.2. Sensitivity analysis of limit cycle models

For oscillatory systems, most dynamic biological data are concerned with how the period of oscillation is affected by a permanent change in parameter values [19, 53], or how the phase or amplitude of oscillation is affected by temporary changes in state variable concentrations or parameter values [12, 79–81]. Sensitivity analysis of dynamical systems is primarily concerned with how a solution varies with respect to perturbations in initial state or parameter values, and these biological quantities may be described within a sensitivity analysis framework.

Biologically relevant sensitivity metrics include: phase change in response to a state perturbation (for example, the one-time addition of a clock protein) $\frac{d\phi}{dx}$; phase change in response to a temporary parameter perturbation (for example, applying a light pulse to photosensitive cells) $\frac{d}{dt}\frac{d\phi}{dp}$; amplitude change in response to a state perturbation $\frac{dA}{dx}$; amplitude change in response to a temporary parameter perturbation $\frac{d}{dt}\frac{dA}{dp}$; period change in response to a permanent parameter change (for example, knockout of a clock protein isoform) $\frac{d\tau}{dp}$. The phase shift $\Delta\phi$ for a temporary change in parameter value converges asymptotically in time. However, because period τ and orbit $\mathbf{x}^\gamma$ are dependent on parameterization, a permanent change in parameter value will result in the phase change $\Delta\phi$ accumulating [22, 23]. The phase response of a system to state or parameter perturbations occurring at different phases is commonly called a phase response curve (PRC), and its amplitude equivalent may be called an amplitude response cure (ARC).

By combining these sensitivity metrics with biological investigations, mathematical models may be used to guide experimentation, predict system behavior under new conditions, identify the roles of novel genes within the biological circuit, or uncover the mechanisms of drug action. In section 4, we additionally show how the infinitesimal parametric phase response curve $\frac{d}{dt}\frac{d\phi}{dp}$ may be used to exert control over the circadian system.

3.3. Analysis of cellular populations

Thus far, we have treated the circadian clock as a single deterministic limit cycle oscillator. This limit cycle oscillator may be interpreted as representing the population-scale circadian oscillation, or alternately the oscillation within a single cell. Physically, each cell contains a noisy oscillator, which exhibits both intrinsic and extrinsic stochasticity. In some cases, simultaneously examining population-scale and single-cell dynamics through mathematical analysis of a population of limit cycle oscillators allows further insight into clock function or control.

In the SCN, coherent population-scale oscillation is self-sustained, due to intercellular communication driving synchrony [9]. In peripheral tissues, however, the lack of paracrine signalling results in a gradual damping of population-scale oscillation, as the cells comprising the population require external signals to maintain a synchronized phase [60]. Cultured circadian reporter cells similarly lack intercellular signalling, thus these cultures must be examined through the dual lens of population and single-cell effects. For example, a temporary pertur-

bation to cultured reporter cells such as a light pulse will have two effects on the amplitude of bioluminescence: a cellular-scale effect due to the deviation from the limit cycle, and a population-scale effect due to the condensing or dispersing of cellular phases [78, 82, 83]. The single-cell effect will be transient, due to relaxation to the limit cycle, but the population synchrony effect will persist well after the pulse has ended.

These effects may be quantified through the use of previously-discussed sensitivity metrics. For example, a perturbation to cells within a region of negative slope of the single-cell PRC will result in increased population synchrony and thus increased population amplitude, whereas a positive slope will decrease population synchrony. Thus, the slope of the single-cell PRC dictates the angle of entrainment for a population of oscillators. Computational methods have been developed to distinguish between single-cell and population-scale effects on amplitude and phase, and a derivation of these methods is provided in section 3.5 [78].

3.4. Mathematical treatment and sensitivity analysis for limit cycle models

In this section, we provide derivations for the calculation of period, phase, and amplitude sensitivity, as introduced in 3.2. We begin by defining a local, first-order sensitivity matrix $\mathbf{S}$ as:

$$s_{i,j}(t,\boldsymbol{\alpha}) = \frac{\partial x_i(t,\boldsymbol{\alpha})}{\partial \alpha_j} = \lim_{\epsilon\to 0} \frac{x_i(t,\boldsymbol{\alpha}+\epsilon\mathbf{e_j}) - x_i(t,\boldsymbol{\alpha})}{\epsilon} \tag{6}$$

where $\boldsymbol{\alpha}$ may be any linear combination of model parameters and/or initial conditions, and $\mathbf{e}_j$ is the jth unit vector [22, 23]. The sensitivity matrix with respect to state initial conditions, $\mathbf{S_x} \in \mathbb{R}^{n\times n}$, may be computed directly, by integrating

$$\frac{d\mathbf{S_x}(t)}{dt} = \mathbf{J}(\mathbf{x}(t))\mathbf{S_x}(t) + \frac{\partial \mathbf{f}(\mathbf{x}(t),\mathbf{p})}{\partial \mathbf{x}(0)}, \tag{7}$$

where $\mathbf{J} \in \mathbb{R}^{n\times n}$ is the Jacobian matrix with element $J_{k,i} = \frac{\partial f_k(\mathbf{x}(t),\mathbf{p})}{\partial x_i}$ and with initial condition $\mathbf{S_x}(0) = \mathbf{I}$, the $n \times n$ identity matrix [85]. The parametric sensitivity matrix (denoted $\mathbf{S_p} \in \mathbb{R}^{n\times m}$) may be solved similarly, by integrating

$$\frac{d\mathbf{S_p}(t)}{dt} = \mathbf{J}(\mathbf{x}(t))\mathbf{S_p}(t) + \frac{\partial \mathbf{f}(\mathbf{x}(t),\mathbf{p})}{\partial \mathbf{p}}, \tag{8}$$

with zero initial condition [23, 85]. In some cases, the direct solution of $\mathbf{S}$ may not be practical, and an alternate formulation using a Green's function approach yields advantages [85].

The parametric period sensitivity $\frac{d\tau}{d\mathbf{p}}$ may be calculated by solving the boundary value problem:

$$\begin{bmatrix} \mathbf{M}-\mathbf{I} & \mathbf{f}(\mathbf{x}_0^\gamma,\mathbf{p}) \\ \frac{\partial f_i(\mathbf{x}_0^\gamma),\mathbf{p})}{\partial \mathbf{x}} & 0 \end{bmatrix} \begin{bmatrix} \mathbf{S_{p,0}} \\ \frac{d\tau}{d\mathbf{p}} \end{bmatrix} = \begin{bmatrix} -\mathbf{S_p}(\tau) \\ -\frac{\partial f_i(\mathbf{x}_0^\gamma),\mathbf{p})}{\partial \mathbf{p}} \end{bmatrix}. \tag{9}$$

Here, $\mathbf{M}$ is the monodromy matrix of the sensitivity system parameterized by $\mathbf{p}$, $\mathbf{I}$ is the $n \times n$ identity matrix, and $\mathbf{S_p}(\tau)$ is the solution to Eq. 8 integrated to time τ from initial condition $\mathbf{0}$. Solving this system yields the desired period sensitivities as well as the initial conditions for parametric sensitivities $\mathbf{S_{p,0}}$. For a detailed derivation of this result, we refer the reader to Ref. [23].

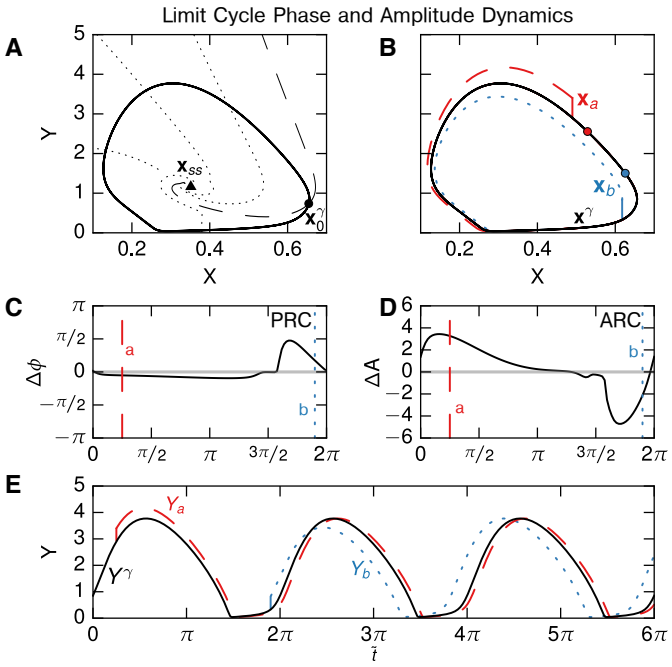

Figure 2: Phase and amplitude response curves for a single two-state limit cycle oscillator model (from [84]) describing oscillator response to perturbation. (**A**) Phase breakdown of state space, as visualized through isochrons: sets of points with constant phase within state-space [10]. The isochron with phase $\phi = 0$ is shown as the dashed line, with each subsequent (dotted) isochron at intervals of $\frac{\tau}{5}$. The fixed point ($\mathbf{x}_{ss}$) and reference point on the limit cycle ($\mathbf{x}_0^\gamma$) are shown with a triangle and a circle, respectively. (**B**) State-space response to an identical perturbation $\Delta\mathbf{x}$ to $\mathbf{x}^\gamma$ at phases $\phi = 0.125\tau$ (trajectory $\mathbf{x}_a(t)$, dashes) and $\phi = 0.95\tau$ (trajectory $\mathbf{x}_b(t)$, dots). The final phase angle at which each trajectory returns to $\mathbf{x}^\gamma$ are shown by circles, indicating a phase delay for a and phase advance for b. Perturbation a results in an amplitude increase (i.e. is perturbed to the outside of $\mathbf{x}^\gamma$), while b results in a decrease. (**C**) Phase and (**D**) amplitude response curves for the perturbation $\Delta\mathbf{x}$ to $\mathbf{x}^\gamma$. (**E**) Time-domain representation of state Y, demonstrating phase and amplitude responses relative to limit cycle path Y^γ.

3.4.1. Phase response to state and parameter perturbations

Because a limit cycle oscillator is attractive, perturbations away from the limit cycle will eventually return to the closed path $\mathbf{x}^\gamma$. Thus, the concept of phase may be extended to any point within the region of attraction (excluding the stationary point for which $\frac{d\mathbf{x}}{dt} = \mathbf{0}$). The phase $\Phi(\mathbf{x}_a) \in [0,\tau)$ of a point $\mathbf{x}_a$ is equal to the initial phase of the oscillator on $\mathbf{x}^\gamma$ to which $\mathbf{x}_a$ will converge asymptotically in time. That is,

$$\Phi(\mathbf{x}_a) = \arg\min_{\phi} \lim_{t\to\infty} \|\mathbf{x}(t) - \mathbf{x}^\gamma(t-\phi)\|, \tag{10}$$

where $\mathbf{x}(0) = \mathbf{x}_a$. A phase response curve (PRC) may then be calculated by applying an identical perturbation in species concentration or parameter at each phase, and calculating the resulting phase shift $\Delta\phi$. The infinitesimal PRC, the response to infinitesimal perturbations in species concentration or parameter value, is defined in [22] for species i:

$$\frac{d\phi}{dx_i} = \lim_{\Delta x_i\to 0} \frac{\Delta\phi}{\Delta x_i}, \tag{11}$$

or for parameter j:

$$\frac{d}{dt}\frac{d\phi}{dp_j} = \lim_{t_p,\Delta p_j\to 0}\frac{\Delta\phi}{t_p\Delta p_j}, \tag{12}$$

where t_p is the duration of the parameter perturbation. Usefully, these quantities are related [22]:

$$\frac{d}{dt}\frac{d\phi}{dp_j} = \frac{d}{dt}\frac{d\phi}{d\mathbf{x}}\frac{d\mathbf{x}}{dp_j} = \frac{d\phi}{d\mathbf{x}}\frac{d\mathbf{f}}{dp_j}, \tag{13}$$

necessitating only the calculation of the state impulse PRC. This may be done through solving Eq. 7 using its Green's function formulation [85]. The homogeneous problem[2] is

$$\frac{d}{dt}\mathbf{K}(t,t') = \mathbf{J}(\mathbf{x}^\gamma(t))\mathbf{K}(t,t'), \tag{14}$$

with $t > t'$ and initial condition $\mathbf{K}(t',t') = \mathbf{I}$, which admits the n linearly-independent solutions to Eq. 7 as the columns of the kernel $\mathbf{K}$. Since $t' \le t$, an adjoint strategy is simpler than solving the integral form of Eq. 14 [86]:

$$\frac{d}{dt'}\mathbf{K}^*(t',t) = -\mathbf{K}^*(t',t)J(\mathbf{x}^\gamma(t')), \quad \mathbf{K}^*(t,t) = I, \quad t' \le t. \tag{15}$$

This system may integrated backwards from $t' = t$ to $t' = 0$ to solve for the adjoint matrix $\mathbf{K}^*$. The infinitesimal PRC is then found from:

$$\frac{d\phi}{dx_i} = \lim_{t\to\infty}\frac{K^*_{ki}(t',t)}{dx^\gamma_k(t)/dt'}, \tag{16}$$

and thus we need only solve for one row of $\mathbf{K}^*$ [22, 86]. In the limit $t \to \infty$, Eq. 16 is τ-periodic as it reaches the limit cycle. In practice, the adjoint solution approaches its limit cycle rapidly and this can be approximated by integration for three periods [22]. We note that as in [22], the sign of this phase shift is chosen to conform to circadian literature. By combining Eqs. 13 and 16, we find the parametric infinitesimal PRC.

3.4.2. Amplitude response to perturbation

Perturbations away from the limit cycle result in changes in oscillatory amplitude $\mathbf{A} \in \mathbb{R}^n$ in addition to phase. Because perturbed trajectories eventually return to $\mathbf{x}^\gamma$, any change in amplitude for a single limit cycle oscillator occurs only in the transient region. We therefore define a reference trajectory $\mathbf{y}(t)$ to be the limit cycle trajectory $\mathbf{x}^\gamma$ shifted to account for the phase at which the perturbation was applied ϕ_0 and the phase shift $\Delta\phi$ resulting from the perturbation:

$$\mathbf{y}(t) = \mathbf{x}^\gamma(t + \phi_0 + \Delta\phi) \tag{17}$$

For a perturbed trajectory $\mathbf{x}(t)$ which converges to the limit cycle reference trajectory $\mathbf{y}(t)$ as $t \to \infty$, the total amplitude change for state i may be defined as in [78]:

$$\Delta A_i(x_i(t), y_i(t)) = \int_0^\infty (x_i(t) - \mu_i)^2 - (y_i(t) - \mu_i)^2 dt, \tag{18}$$

where μ_i is the mean value of state i:

$$\mu_i = \frac{1}{\tau}\int_0^\tau x_i^\gamma(t)dt. \tag{19}$$

Because $\mathbf{x}(t)$ and $\mathbf{y}(t)$ converge, the function ΔA does as well. An infinitesimal amplitude response curve (ARC) may be defined in an analogous fashion to the infinitesimal PRC:

$$\frac{dA_i}{dx_j} = \int_0^\infty \lim_{\Delta x_j(0)\to 0}\frac{h_i(t)}{\Delta x_j(0)}dt, \tag{20}$$

where $h_i(t)$ is the integrand of Eq. 18. By Taylor expanding in $\Delta\phi$, and substituting terms derived previously [78], we arrive at an exact infinitesimal ARC for each state:

$$\frac{dA_i}{dx_j} = \int_0^\infty 2\left(s_{i,j}(t) - f_i(\mathbf{x}^\gamma(t+\phi_0))\frac{d\phi}{dx_j}\right)(x_i^\gamma(t+\phi_0)) - \mu_i)dt, \tag{21}$$

where $s_{i,j}$ is an element of $\mathbf{S}_\mathbf{x}$. The state impulse ARC may then be used to calculate the parameter infinitesimal ARC:

$$\frac{d}{dt}\frac{d\mathbf{A}}{dp_j} = \frac{d\mathbf{A}}{d\mathbf{x}}\frac{d\mathbf{f}}{dp_j}. \tag{22}$$

3.5. Mathematical treatment of limit cycle oscillator populations

A population of oscillators may be treated through a phase-density approach, as is common for phase-only models [78, 83]. Phase-only oscillator models use a single differential equation for the phase of each oscillator within a population, and capture population dynamics through coupling terms in these equations. To maintain consistency with these phase-only approaches, we use the mechanistic limit cycle oscillator formulation for which $\tau = 2\pi$ as defined in Eq. 5. The total number of oscillators is conserved, and phase $\phi \in [0, 2\pi)$, so

$$\int_0^{2\pi} p(\phi,\tilde{t})d\phi = 1. \tag{23}$$

The exact phase probability density function $\hat{p}(\phi,\tilde{t})$ following a perturbation may be calculated exactly by using a change of variables:

$$\hat{p}(\phi,\tilde{t})dg(\phi) = p(\phi,\tilde{t})d\phi, \tag{24}$$

where $p(\phi,\tilde{t})$ is the phase probability density function prior to perturbation, and $g(\phi) = \phi + \Delta\phi$ is the phase transition curve, a mapping of oscillator phase before perturbation to phase following perturbation. However, in the limit of a large oscillator population ($n \to \infty$) it is simpler to map the distribution of phases in the population using a complex variable z, given by

$$\begin{aligned} z &= \rho e^{i\bar{\phi}} \\ &= \frac{1}{N}\sum_{j=1}^{N} e^{i\phi_j}, \end{aligned} \tag{25}$$

where $\bar{\phi}$ is the mean phase and ρ is called the Kuramoto order parameter, also called the synchronization index. The Kuramoto order parameter is related to the population variance and

[2] On notation: we have chosen to use t and t' consistently with [85, 86], but note that our t is the equivalent of T, and our t' is the equivalent of t in [22]. T in [85, 86] refers to the period of oscillation.

yields a simpler calculation at the expense of some detail regarding the exact distribution of phases (for additional detail, see [87]). For a perfectly synchronized population, $\rho = 1$, and for a population uniformly distributed on $[0, 2\pi)$, $\rho = 0$. The population phase and amplitude responses may be then calculated by

$$\Delta\bar{\phi} = \angle z - \angle\hat{z}, \tag{26}$$

and

$$\Delta\rho = |z| - |\hat{z}|, \tag{27}$$

respectively, where

$$z = \int_0^{2\pi} \mathrm{e}^{i\phi} p(\phi, \tilde{t}) d\phi, \tag{28}$$

$$\hat{z} = \int_0^{2\pi} \mathrm{e}^{i\phi} \hat{p}(\phi, \tilde{t}) d\phi = \int_0^{2\pi} \mathrm{e}^{ig(\phi)} p(\phi, \tilde{t}) d\phi. \tag{29}$$

3.5.1. *Phase diffusion of uncoupled oscillators and population-scale mean expression profiles*

Even for an identical population of oscillators, intrinsic cycle-to-cycle variability in period length will effect a gradual desynchronization over time. The drift of phases due to stochastic noise is approximately diffusive [20, 78, 88, 89], and so the evolution of the phase probability density function may be described through a Fokker-Planck equation:

$$\frac{\partial p}{\partial \tilde{t}} = \frac{\partial p}{\partial \phi} + D\frac{\partial^2 p}{\partial \phi^2}, \tag{30}$$

where $D\frac{\partial^2 p}{\partial \phi^2}$ describes phase diffusion about $[0, 2\pi)$ the with diffusion coefficient D, and $\frac{\partial p}{\partial \phi}$ describes convection of mean phase around $[0, 2\pi)$. Note that Eq. 30 has periodic boundary conditions and an initial condition $p(\phi, 0) = \Psi(\phi)$, yielding the solution as a convolution of the initial conditions with a wrapped normal distribution:

$$p(\phi, \tilde{t}) = \Psi(\phi) * f_{WN}(\phi; \tilde{t}, \sqrt{2D\tilde{t}}), \tag{31}$$

where f_{WN} is the wrapped normal distribution, $\tilde{t}$ is the mean phase, and $\sqrt{2D\tilde{t}}$ is the standard deviation of phase [78]. This convolution may be simplified by approximating $\Psi(\phi)$ as a normal distribution with mean μ_0 and standard deviation σ_0, to yield

$$p(\phi, \tilde{t}) = f_{WN}(\phi; \mu_0 + \tilde{t}, \sqrt{\sigma_0^2 + 2D^2\tilde{t}^2}). \tag{32}$$

The population-scale mean expression of state i, $\bar{x}_i(\tilde{t})$, for oscillators on the limit cycle $\mathbf{x}^\gamma$ can be found through a weighted average of the phase probability density function:

$$\bar{x}_i(\tilde{t}) = \int_0^{2\pi} x_i^\gamma(\phi) p(\phi, \tilde{t}) d\phi. \tag{33}$$

For the case where limit cycle trajectory $x_i^\gamma(\tilde{t}) = \cos(\tilde{t})$, and where the phase probability density function evolves according to the convection-diffusion equation Eq. 30, Eq. 33 yields an exponentially-damped sinusoidal result [78]:

$$\bar{x}_i(t) = \mathrm{e}^{-D\tilde{t}} \cos(\tilde{t}), \tag{34}$$

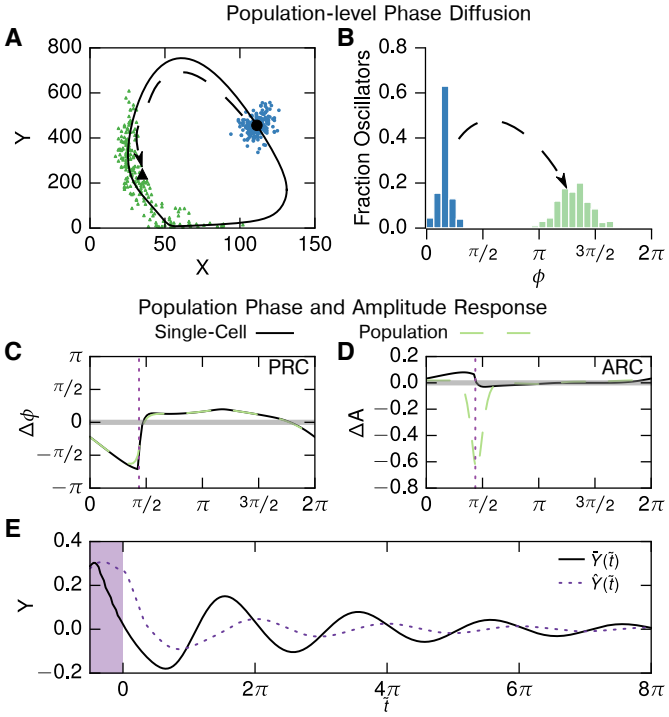

Figure 3: Phase and amplitude response dynamics for a population of two-state limit cycle oscillator models from [84]. (**A**) State-space representation of phase diffusion. An initial population of 200 oscillators (circles, blue) was simulated stochastically for $\frac{\tau}{2}$ resulting in a dispersion of final phases (triangles, green). The average molecular count of X and Y for initial and final conditions are shown in bold. The movement of the center of mass toward the inside of limit cycle orbit $\mathbf{x}^\gamma$ reflects amplitude damping due to desynchronization. (**B**) The diffusion of phases due to intrinsic noise is shown as a histogram of phases for the simulation from panel A. (**C** and **D**) Single-cell (solid line) and population (dashed line) PRC and ARC, for a temporary 40% increase in parameter k_2. (**E**) Population-scale mean expression profile $\hat{Y}(\tilde{t})$ resulting from perturbation at the phase indicated in panels B and C (dotted line in both panels). This results in a phase lag, and a loss of amplitude in comparison to the unperturbed trajectory $\bar{Y}(\tilde{t})$ due to the desynchronizing effect of the pulse, despite negligible changes in single-cell amplitude.

consistent with both experimental and computational studies [21, 57, 60]. Non-sinusoidal limit cycles will also approach this trajectory, as phase diffusion will damp higher frequency sinusoidal components of the limit cycle [78].

The population-scale mean expression after a perturbation may be calculated by decomposing the perturbed trajectory $\hat{x}_i(\tilde{t})$ into the steady-state perturbed trajectory $\hat{x}_{i,SS}$ resulting from the condensing or dispersing of phases along the limit cycle, and the transient population-scale deviations from the limit cycle $\hat{x}_{i,trans}$ which eventually converge to 0. The steady-state trajectory is

$$\hat{x}_{i,SS}(\tilde{t}) = \int_0^{2\pi} x_i^\gamma(\phi) \hat{p}(\phi, \tilde{t}) d\phi, \tag{35}$$

where $\hat{p}(\phi, \tilde{t})$ must be calculated numerically for short times immediately following the perturbation, but may be approximated by Eq. 29 for sufficient damping. The transient trajectory necessitates the definition of the deviation trajectory:

$$\delta x_i(\phi, \tilde{t}) = x_i(\tilde{t}) - x_i^\gamma(\tilde{t} + \phi + \Delta\phi), \tag{36}$$

which represents the distance between the perturbed trajectory and its reference after convergence to the limit cycle. The average transient affect can then be calculated by weighting the deviation term by the phase probability density prior to perturbation:

$$\hat{x}_{i,trans}(\tilde{t}) = \int_0^{2\pi} \delta x_i(\phi, \tilde{t}) p(\phi, \tilde{t}) d\phi. \tag{37}$$

Finally, the population-scale mean expression profile, $\hat{x}_i(\tilde{t})$, is

$$\hat{x}_i(\tilde{t}) = \int_0^{2\pi} \left(x_i^{\gamma}(\phi) \hat{p}(\phi, \tilde{t}) + \delta x_i(\phi, \tilde{t}) p(\phi, \tilde{t}) \right) d\phi, \tag{38}$$

as in [78].

4. Taking control of the clock

Oscillators are a common biological motif, and processes such as neuronal firing, P53 oscillations, breathing, and the heartbeat may be modeled using limit cycle dynamics [90]. Prior studies have analyzed several of these systems under the lens of control theory including glycolytic oscillators [91], the drosophila circadian clock [27, 91–93], and the light-responsive human clock [28, 29]. Leveraging computational models of the circadian clock and the tools outlined in the prior section, it is possible to formulate feedback controllers for the manipulation of clock phase, clock amplitude, or entrainment. Fig. 4 shows a simple control scheme by which this may be accomplished. In general, such a control system consists of a sensor tasked with observing the system state, an actuator by which control is exerted, and a control algorithm connecting these parts. Herein, we briefly discuss the components of a model predictive control (MPC) strategy and provide an example of using MPC-guided administration of a small-molecule pharmaceutical to the shift circadian phase of a single oscillator.

4.1. Sensor design

A critical component of a circadian control system is the design of a sensor which can accurately assess circadian phase while remaining minimally invasive. Current markers of human circadian phase are plasma or saliva melatonin, plasma cortisol, or core body temperature [94]. More recent works have utilized ambulatory monitoring approaches, using variables such as motion, respiration, light exposure, and ECG, and fitting a multivariate model, with some success [95]. However, these current approaches are likely too invasive for everyday use. Furthermore, single-dimensional recordings such as melatonin provide limited resolution for tracking phase, such as during daytime when melatonin concentration is negligible. Enabled by smartphone technology, another possible route to sensing circadian phase would be actigraphy in conjunction with a calculated light schedule [96]. However, these metrics would necessitate a robust control algorithm to compensate for potential sensor error. In general, the performance of any control algorithm would be highly subject to sensor accuracy, and choice of a sensor remains an open research question.

4.2. Actuator design

4.2.1. Photic actuation

The most common route to artificial control of the clock is through the natural control variable: light. This path is favorable as it is non-invasive and the mechanistic pathway is relatively well-understood. Historically, many studies have examined the role of light in entraining the clock. Recent studies have also begun to examine closing the loop between sensing and control of the clock by calculating an optimal light profile for reentrainment [28, 96]. Potential downsides to using light in clock control include delays in responsiveness, as the system is not evolutionarily optimized to respond to large shifts in phase rapidly; and loss of control during "dead zones," where light has little effect on circadian phase [30].

4.2.2. Pharmacological actuation

Small-molecule modulators of the circadian clock have gained significant recent attention [19, 97, 98]. Small-molecule pharmaceuticals are attractive due to facile delivery and uptake and ability to target specific proteins or complexes within the clock. Two such molecules, KL001 and Longdaysin, have been identified via high-throughput screening methods. Identifying the mechanistic action of these clock modulators presents a unique challenge, due to the inherent complexity of the gene regulatory network obscuring the direct effect. Neurotransmitters, or pharmaceuticals which modulate neurotransmitter expression, offer another possible path to control of the circadian oscillator. In particular, the neurotransmitters VIP and GABA have attracted attention, due to their preeminent role in synchronizing the SCN [99, 100]. However, these neurotransmitters are also implicated in a variety of non-circadian functions, and may not be sufficiently precise to target solely the clock. An important limitation on the potential of molecular clock modulators is that the oscillator appears to be optimized for high-amplitude high-precision rhythms, and very few clock modulations are able to simultaneously increase amplitude and precision for an extended duration [60]. This suggests that any long-term (i.e. many-cycle) clock modulation might be best accomplished by a dynamic approach, where circadian amplitudes are increased by precisely timing the administration of a clock-modulating therapeutic.

4.3. Algorithm example: MPC phase resetting of the circadian clock

Circadian disruptions such as jet lag and shift work involve large phase-shifts of the clock, which may occur over many days. Here, we used the clock model and small molecule KL001 response mechanism developed in Refs. [19, 98] to reentrain the circadian clock following an environmental shift. MPC is ideally suited for this problem for several reasons: (i) models describing the mechanistic action of KL001 have been developed and validated, (ii) MPC is robust to noise and plant-model mismatch, and (iii) MPC employs short horizons to reduce its computational cost.

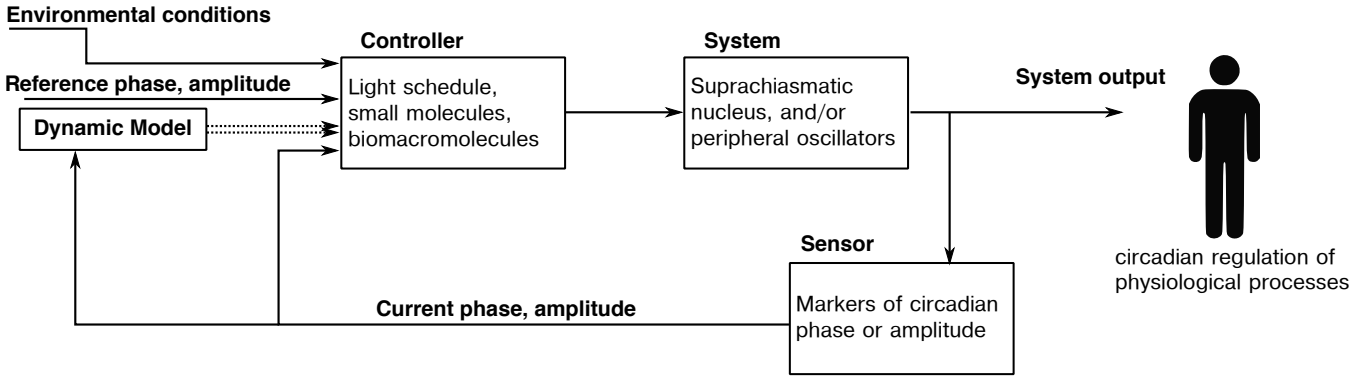

Figure 4: A generalized scheme for feedback control of the circadian clock identifying essential components and possible control variables. This diagram is generalizable to a variety of desirable control outcomes (optimal entrainment, phase shifting, amplitude) and control vectors (light, pharmaceuticals). A feed-forward scheme could be similarly implemented by shifting the clock in anticipation of a disturbance, such as light exposure during night.

Optimal control provides another path to control of the circadian oscillator, however, formulating and solving the two-point boundary value problem remains a significant computational challenge. Prior studies have formulated these as mixed-integer optimal control problems, yielding a reduction in computational complexity, though this remains prohibitively computationally expensive [91, 93]. Alternate control implementations could be evaluated by comparing the time required to perform phase shifts for a variety of desired shifts and initial conditions. The following MPC implementation is basic, and will form the basis for future investigations.

4.3.1. Model formulation

To simulate the effect of KL001 on clock function, we selected a deterministic and mechanistic limit cycle model, with ODEs describing the kinetics of the negative feedback loop of the core clock [19]. States included in this model are *Per*, *Cry1*, and *Cry2* mRNAs; PER, CRY1, and CRY2 cytosolic proteins; and PER-CRY1, and PER-CRY2 nuclear transcription factors. We selected this model as it was originally conceived to capture the behavior of KL001 mechanistically. The complete equations and parameterization for this model are included in the Supplement.

KL001 is known to slow the degradation rate of nuclear CRY in a dose-dependent fashion through the FBXL3-CRY pathway. This effect is achieved *in silico* by a decrease in parameter *vdCn* of the model from Ref. [19], resulting in stabilization of nuclear CRYs [98]. Because the pharmacodynamics of KL001 are not yet established, we use a negative perturbation to parameter *vdCn* as our single control target, and bound control input $u_{vdCn} \in [0, vdCn]$ to conform to physical reality. Thus, Model 1 of Ref. [98] is adjusted, such that:

$$\begin{aligned}\frac{d\mathbf{C1N}}{dt} &= v_{\mathrm{a},\mathbf{CP}}\ \mathbf{P}\ \mathbf{C1} - v_{\mathrm{d},\mathbf{CP}}\ \mathbf{C1N} \\ &\quad - \frac{(vdCn - u)\ \mathbf{C1N}}{k_{\mathrm{deg},\mathbf{Cn}} + \mathbf{C1N} + \mathbf{C2N}},\end{aligned} \tag{39}$$

and

$$\begin{aligned}\frac{d\mathbf{C2N}}{dt} &= v_{\mathrm{a},\mathbf{CP}}\ \mathbf{P}\ \mathbf{C2} - v_{\mathrm{d},\mathbf{CP}}\ \mathbf{C2N} \\ &\quad - \frac{(vdCn - u)\ m_{\mathbf{C2N}}\ \mathbf{C2N}}{k_{\mathrm{deg},\mathbf{Cn}} + \mathbf{C2N} + \mathbf{C1N}},\end{aligned} \tag{40}$$

where u is the discretized control input. Eqns. 39 and 40 describe the dynamics of nuclear PER-CRY1 and PER-CRY2, with the first two terms in each describing the reversible dimerization process of CRY1 (**C1**) and CRY2 (**C2**) with PER (**P**). It is assumed that when these dimers form, they immediately enter the nucleus, hence the positive effect on nuclear PER-CRY1 and PER-CRY2 (**C1N** and **C2N**). The final term in Eqns. 39 and 40 describes the shared, enzyme-mediated degradation of nuclear PER-CRY1 and PER-CRY2. Thus, the reduction in *vdCn* decreases the rate of degradation and stabilizes these proteins. Alternate or additional control inputs could be used, and could potentially be selected via identifying the most sensitive physical parameters [27].

Rather than applying MPC to the full model, we applied MPC to the phase ϕ of the system where the phase was assumed to evolve during each time step i according to:

$$\hat{\phi}_{m,i+1} = \phi_{a,i} + \frac{2\pi(t_{i+1} - t_i)}{\tau} + \int_{t_i}^{t_{i+1}} -u_i \frac{d}{dt}\frac{d\phi}{d(vdCn)}dt, \tag{41}$$

where $\phi_{a,i}$ is the current phase of the system, and $\hat{\phi}_{m,i+1}$ is the predicted phase at the next time step according to the model in Eq. 41. This simplification is achieved by applying the formulation of infinitesimal parameter phase response in Eq. 13. Implicitly, this assumes that oscillators with identical phase (i.e. on an isochron) respond identically to perturbation regardless of distance from the limit cycle. This assumption holds for oscillators reasonably close to the limit cycle, but will fail near the phase singularity present at the center of the limit cycle.

4.3.2. Optimization of control action

The optimal re-entrainment of this model following a shift may then be found via MPC with a prediction horizon of one.

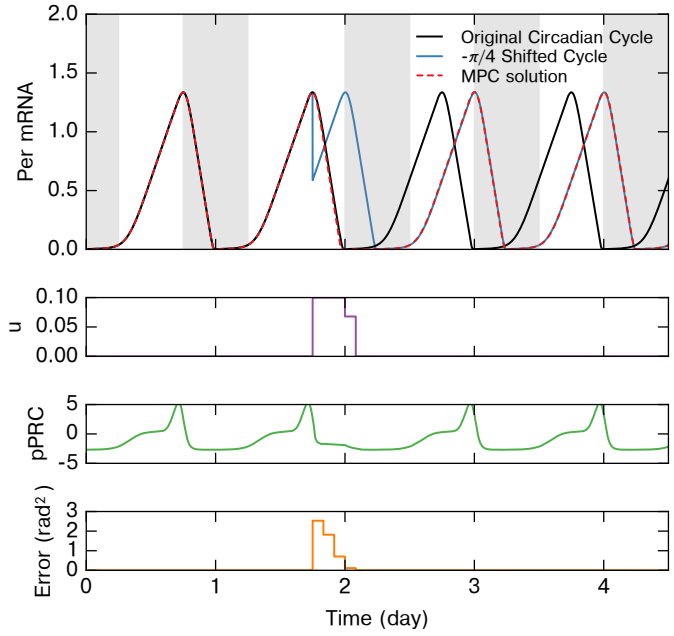

Figure 5: MPC using KL001 allows rapid re-entrainment of the clock following a 6 hour phase delay. The original clock trajectory is shown in black, and the trajectory mapping the instantaneous environmental time is shown in blue. The MPC solution is shown as a dashed red line. The transition to the new light cycle is made in its entirety in 14 hours, and is accomplished by suppressing nuclear CRY degradation, and indirectly *Per* transcription, delaying the onset of the new cycle. Dark bars visualize local night, between 18:00 and 06:00 environmental time. Bottom plots show the discrete control trajectory $u(t)$, the parametric PRC for u, and the phase error at each time segment, respectively, in two hour intervals.

Put simply, the algorithm consists of calculating the phase of the system (Model 1 from [98]) at t_i, computing the optimal control input so as to minimize the difference between the predicted system phase (Eq. 41) and reference environmental phase at t_{i+1}, then applying that input to the system for the ensuing control period. This is repeated for N_i steps throughout the simulation. The size of each step for the prediction horizon and control discretization was set to two hours, for an oscillator with a period of exactly 24 hours. The optimal control step $u_i^\star$ was selected by minimizing:

$$J = w_\phi(\phi_{m,i+1}(u_i) - \phi_{r,i+1})^2 + w_u u_i^2, \tag{42}$$

where w_ϕ and w_u are positive scalar weights, and $\phi_{r,i+1}$ is the reference phase of the external environment at the next time point. Upon computing the optimal control action $u^\star$, we implement this on the continuous time plant, Model 1 in [98].

The MPC problem was formulated and solved in the Python language. The phase response curve $\frac{d}{dt}\frac{d\phi}{d(vdCn)}$ was calculated using tools from the CasADi automatic differentiation package [101]. The MPC problem was formulated using the LSODA integration routine through the SciPy interface [102], and the optimal control step was selected using particle swarm optimization via the PySwarm package. Because the predictive horizon is a single step for this simple example, the complete simulation may be computed in several minutes. For this example, weights w_ϕ and w_u were set to 1.0 and 0.1, respectively.

This algorithm was applied for a phase delay of 6 hours occurring at 18:00 on the second day of simulation, as shown in Fig. 5. This scenario corresponds with a flight from Paris to Boston, though we do not take light effects into account for this simple example. By suppressing degradation of PER-CRY nuclear heterodimers, the optimal KL001 dosage is able to delay the onset of *Per* activation, and rapidly shift the clock to the new environmental phase. Notably, because KL001 functions primarily to slow the clock, phase advances take several cycles to complete in the absence of an additional entraining force. This is evident from the asymmetry in the parametric PRC for *vdCn* shown in Fig. 5, where a much larger region of the PRC is negative. A multi-target control may be more effective for shifting the clock symmetrically [27]. Because the control algorithm was applied to a simplification of the more complex plant and then tested on the plant itself, we show that this method is robust to a degree of plant-model mismatch.

5. Conclusions

The mammalian circadian system is a natural, multi-scale, robust control system with widespread influence over metabolism and behavior. In the past two decades, a systems engineering approach has yielded great insight into the mechanistic function of the mammalian circadian oscillator. As technology for sensing and actuating circadian function continues to develop, control theory also will play an important role in developing novel clock therapies. Furthermore, design principles for generating stable control from sloppy biological components may yield improvements in the design of artificial control strategies, or in the design of artificial genetic circuits in synthetic biology.

Acknowledgements

We thank Stamatina Zavitsanou, Ankush Chakrabarty, Sunil Deshpande, and Ravi Gondhalekar, Peter C. St. John, and Kelsey Dean for helpful discussions. We especially thank Ankush Chakrabarty for a critical reading of the manuscript, and Peter C. St. John for open-source code and data. We also thank Steve A. Kay, Erik D. Herzog, and Linda R. Petzold for biological and mathematical insight into this system, and for their extensive experimental and theoretical collaborations leading to this work.

This work was funded by the National Institutes of Health (NIH) awards T32-HLO7901 (J.H.A.), and R01-GM096873-01 (F.J.D.).

References

[1] S. M. Reppert, D. R. Weaver, Coordination of circadian timing in mammals, Nature 418 (6901) (2002) 935–941.

[2] P. E. Hardin, The circadian timekeeping system of drosophila, Curr. Biol. 15 (17) (2005) R714–R722.

[3] S. L. Harmer, J. B. Hogenesch, M. Straume, H. S. Chang, B. Han, T. Zhu, X. Wang, J. A. Kreps, S. A. Kay, Orchestrated transcription of key pathways in arabidopsis by the circadian clock, Science 290 (5499) (2000) 2110–2113.

[4] J. C. Dunlap, The neurospora circadian system, J. Biol. Rhythms 19 (5) (2004) 414–424.

[5] M. Ishiura, S. Kutsuna, S. Aoki, H. Iwasaki, C. R. Andersson, A. Tanabe, S. S. Golden, C. H. Johnson, T. Kondo, Expression of a gene cluster kaiabc as a circadian feedback process in cyanobacteria, Science 281 (5382) (1998) 1519–1523.

[6] M. Nakajima, K. Imai, H. Ito, T. Nishiwaki, Y. Murayama, H. Iwasaki, T. Oyama, T. Kondo, Reconstitution of circadian oscillation of cyanobacterial kaic phosphorylation in vitro, Science 308 (5720) (2005) 414–415.

[7] J. C. Dunlap, Molecular bases for circadian clocks, Cell 96 (2) (1999) 271–290.

[8] J. S. O'Neill, G. van Ooijen, L. E. Dixon, C. Troein, F. Corellou, F.-Y. Bouget, A. B. Reddy, A. J. Millar, Circadian rhythms persist without transcription in a eukaryote, Nature 469 (7331) (2011) 554–558.

[9] D. K. Welsh, J. S. Takahashi, S. A. Kay, Suprachiasmatic nucleus: cell autonomy and network properties, Annu. Rev. Physiol. 72 (2010) 551–577.

[10] F. J. Doyle III, R. Gunawan, N. Bagheri, H. Mirsky, T. L. To, Circadian rhythm: A natural, robust, multi-scale control system, Comput. Chem. Eng. 30 (10-12) (2006) 1700–1711.

[11] R. E. Kronauer, D. B. Forger, M. E. Jewett, Quantifying human circadian pacemaker response to brief, extended, and repeated light stimuli over the phototopic range, J. Biol. Rhythms 14 (6) (1999) 500–515.

[12] M. E. Jewett, D. B. Forger, R. E. Kronauer, Revised limit cycle oscillator model of human circadian pacemaker, J. Biol. Rhythms 14 (6) (1999) 493–500.

[13] J.-C. Leloup, A. Goldbeter, Toward a detailed computational model for the mammalian circadian clock, Proc. Natl. Acad. Sci. U. S. A. 100 (2003) 7051–7056.

[14] D. Gonze, J. Halloy, J.-C. Leloup, A. Goldbeter, Stochastic models for circadian rhythms: effect of molecular noise on periodic and chaotic behaviour, C. R. Biol. 326 (2) (2003) 189–203.

[15] D. B. Forger, C. S. Peskin, Stochastic simulation of the mammalian circadian clock, Proc. Natl. Acad. Sci. U. S. A. 102 (2) (2005) 321–324.

[16] T.-L. To, M. A. Henson, E. D. Herzog, F. J. Doyle III, A molecular model for intercellular synchronization in the mammalian circadian clock, Biophys. J. 92 (11) (2007) 3792–3803.

[17] H. P. Mirsky, A. C. Liu, D. K. Welsh, S. A. Kay, F. J. Doyle III, A model of the cell-autonomous mammalian circadian clock, Proc. Natl. Acad. Sci. U. S. A. 106 (27) (2009) 11107–11112.

[18] C. H. Ko, Y. R. Yamada, D. K. Welsh, E. D. Buhr, A. C. Liu, E. E. Zhang, M. R. Ralph, S. A. Kay, D. B. Forger, J. S. Takahashi, Emergence of noise-induced oscillations in the central circadian pacemaker, PLoS Biol. 8 (10) (2010) e1000513.

[19] T. Hirota, J. W. Lee, P. C. St. John, M. Sawa, K. Iwaisako, T. Noguchi, P. Y. Pongsawakul, T. Sonntag, D. K. Welsh, D. A. Brenner, F. J. Doyle III, P. G. Schultz, S. A. Kay, Identification of small molecule activators of cryptochrome, Science 337 (6098) (2012) 1094–1097.

[20] D. Gonze, A. Goldbeter, Circadian rhythms and molecular noise, Chaos 16 (2) (2006) 026110.

[21] J. Rougemont, F. Naef, Dynamical signatures of cellular fluctuations and oscillator stability in peripheral circadian clocks, Mol. Syst. Biol. 3 (93) (2007) 93.

[22] S. R. Taylor, R. Gunawan, L. R. Petzold, F. J. Doyle III, Sensitivity measures for oscillating systems: Application to mammalian circadian gene network, IEEE Trans. Automat. Contr. 53 (2008) 177–188.

[23] A. Wilkins, B. Tidor, J. White, P. Barton, Sensitivity analysis for oscillating dynamical systems, SIAM J. Sci. Comput. 31 (4) (2009) 2706–2732.

[24] P. C. St. John, F. J. Doyle III, Estimating confidence intervals in predicted responses for oscillatory biological models, BMC Syst. Biol. 7 (2013) 71.

[25] S. R. Taylor, A. Cheever, S. M. Harmon, Velocity response curves demonstrate the complexity of modeling entrainable clocks, J. Theor. Biol. 363 (2014) 307–317.

[26] N. Bagheri, S. R. Taylor, K. Meeker, L. R. Petzold, F. J. Doyle III, Synchrony and entrainment properties of robust circadian oscillators, J. R. Soc. Interface 5 (Suppl_1) (2008) S17–S28.

[27] N. Bagheri, J. Stelling, F. J. Doyle III, Circadian phase resetting via single and multiple control targets, PLoS Comput. Biol. 4 (7).

[28] K. Serkh, D. B. Forger, Optimal schedules of light exposure for rapidly correcting circadian misalignment, PLoS Comput. Biol. 10 (4) (2014) e1003523.

[29] J. Zhang, W. Qiao, J. T. Wen, A. Julius, Light-based circadian rhythm control: Entrainment and optimization, Automatica 68 (2016) 44–55.

[30] J. C. Dunlap, J. J. Loros, P. J. DeCoursey, Chronobiology, Sinauer Associates, Inc., 2004.

[31] C. H. Ko, J. S. Takahashi, Molecular components of the mammalian circadian clock, Hum. Mol. Genet. 15 (2) (2006) 271–277.

[32] J. A. Mohawk, C. B. Green, J. S. Takahashi, Central and peripheral circadian clocks in mammals, Annu. Rev. Neurosci. 35 (1) (2012) 445–462.

[33] K. A. Lamia, K.-F. Storch, C. J. Weitz, Physiological significance of a peripheral tissue circadian clock, Proc. Natl. Acad. Sci. U. S. A. 105 (39) (2008) 15172–15177.

[34] S. Panda, M. P. Antoch, B. H. Miller, A. I. Su, A. B. Schook, M. Straume, P. G. Schultz, S. a. Kay, J. S. Takahashi, J. B. Hogenesch, Coordinated transcription of key pathways in the mouse by the circadian clock, Cell 109 (3) (2002) 307–320.

[35] H. R. Ueda, W. Chen, A. Adachi, H. Wakamatsu, S. Hayashi, T. Takasugi, M. Nagano, K.-i. Nakahama, Y. Suzuki, S. Sugano, M. Iino, Y. Shigeyoshi, S. Hashimoto, A transcription factor response element for gene expression during circadian night, Nature 418 (6897) (2002) 534–539.

[36] K.-A. Stokkan, Entrainment of the circadian clock in the liver by feeding, Science 291 (5503) (2001) 490–493.

[37] C. B. Green, J. S. Takahashi, J. Bass, The meter of metabolism, Cell 134 (5) (2008) 728–742.

[38] P. L. Lowrey, J. S. Takahashi, Mammalian circadian biology: elucidating genome-wide levels of temporal organization, Annu. Rev. Genomics Hum. Genet. 5 (47) (2004) 407–441.

[39] B. Marcheva, K. M. Ramsey, E. D. Buhr, Y. Kobayashi, H. Su, C. H. Ko, G. Ivanova, C. Omura, S. Mo, M. H. Vitaterna, J. P. Lopez, L. H. Philipson, C. A. Bradfield, S. D. Crosby, L. JeBailey, X. Wang, J. S. Takahashi, J. Bass, Disruption of the clock components clock and bmal1 leads to hypoinsulinaemia and diabetes, Nature 466 (7306) (2010) 627–631.

[40] M. Hatori, C. Vollmers, A. Zarrinpar, L. DiTacchio, E. A. Bushong, S. Gill, M. Leblanc, A. Chaix, M. Joens, J. A. Fitzpatrick, M. H. Ellisman, S. Panda, Time-restricted feeding without reducing caloric intake prevents metabolic diseases in mice fed a high-fat diet, Cell Metab. 15 (6) (2012) 848–860.

[41] H. C. Chang, L. Guarente, Xsirt1 mediates central circadian control in the scn by a mechanism that decays with aging, Cell 153 (7) (2013) 1448–1460.

[42] A. Pan, E. S. Schernhammer, Q. Sun, F. B. Hu, Rotating night shift work and risk of type 2 diabetes: Two prospective cohort studies in women, PLoS Med. 8 (12).

[43] A. Mukherji, A. Kobiita, M. Damara, N. Misra, H. Meziane, M.-F. Champy, P. Chambon, Shifting eating to the circadian rest phase misaligns the peripheral clocks with the master scn clock and leads to a metabolic syndrome, Proc. Natl. Acad. Sci. 112 (48) (2015) E6691–E6698.

[44] K. Wulff, S. Gatti, J. G. Wettstein, R. G. Foster, Sleep and circadian rhythm disruption in psychiatric and neurodegenerative disease, Nat. Rev. Neurosci. 11 (8) (2010) 589–599.

[45] R. Yehuda, M. H. Teicher, R. L. Trestman, R. A. Levengood, L. J. Siever, Cortisol regulation in posttraumatic stress disorder and major depression: A chronobiological analysis, Biol. Psychiatry 40 (2) (1996) 79–88.

[46] A. M. Rosenwasser, Circadian clock genes: Non-circadian roles in sleep, addiction, and psychiatric disorders?, Neurosci. Biobehav. Rev. 34 (8) (2010) 1249–1255.

[47] B. Lemmer, Circadian rhythms and drug delivery, J. Control. Release 16 (1-2) (1991) 63–74.

[48] F. Lévi, A. Okyar, S. Dulong, P. F. Innominato, J. Clairambault, Circadian timing in cancer treatments, Annu. Rev. Pharmacol. Toxicol. 50 (1) (2010) 377–421.

[49] J. S. O'Neill, A. B. Reddy, Circadian clocks in human red blood cells, Nature 469 (7331) (2011) 498–503.

[50] R. Ye, C. P. Selby, N. Ozturk, Y. Annayev, A. Sancar, Biochemical analysis of the canonical model for the mammalian circadian clock, J. Biol. Chem. 286 (29) (2011) 25891–25902.
[51] P. Emery, S. M. Reppert, A rhythmic ror, Neuron 43 (4) (2004) 443–446.
[52] H. R. Ueda, S. Hayashi, W. Chen, M. Sano, M. Machida, Y. Shigeyoshi, M. Iino, S. Hashimoto, System-level identification of transcriptional circuits underlying mammalian circadian clocks, Nat. Genet. 37 (2) (2005) 187–192.
[53] E. E. Zhang, A. C. Liu, T. Hirota, L. J. Miraglia, G. Welch, P. Y. Pongsawakul, X. Liu, A. Atwood, J. W. Huss, J. Janes, A. I. Su, J. B. Hogenesch, S. A. Kay, A genome-wide rnai screen for modifiers of the circadian clock in human cells, Cell 139 (1) (2009) 199–210.
[54] B. C. Goodwin, Oscillatory behavior in enzymatic control processes, Adv. Enzyme Regul. 3 (1965) 425–437.
[55] M. B. Elowitz, A. J. Levine, E. D. Siggia, P. S. Swain, Stochastic gene expression in a single cell, Sci. Signal. 297 (5584) (2002) 1183.
[56] E. D. Herzog, S. J. Aton, R. Numano, Y. Sakaki, H. Tei, Temporal precision in the mammalian circadian system: A reliable clock from less reliable neurons, J. Biol. Rhythms 19 (1) (2004) 35–46.
[57] D. K. Welsh, S.-H. Yoo, A. C. Liu, J. S. Takahashi, S. A. Kay, Bioluminescence imaging of individual fibroblasts reveals persistent, independently phased circadian rhythms of clock gene expression, Curr. Biol. 14 (24) (2004) 2289–2295.
[58] N. Barkai, S. Leibler, Circadian clocks limited by noise, Nature 403 (6767) (2000) 267–268.
[59] J. H. Abel, L. A. Widmer, P. C. St. John, J. Stelling, F. J. Doyle III, A coupled stochastic model explains differences in cry knockout behavior, IEEE Life Sci. Lett. 1 (1) (2015) 3–6.
[60] P. C. St. John, F. J. Doyle III, Quantifying stochastic noise in cultured circadian reporter cells, PLOS Comput. Biol. 11 (11) (2015) e1004451.
[61] S.-H. Yoo, S. Yamazaki, P. L. Lowrey, K. Shimomura, C. H. Ko, E. D. Buhr, S. M. Siepka, H.-K. Hong, W. J. Oh, O. J. Yoo, M. Menaker, J. S. Takahashi, Period2::luciferase real-time reporting of circadian dynamics reveals persistent circadian oscillations in mouse peripheral tissues, Proc. Natl. Acad. Sci. U. S. A. 101 (15) (2004) 5339–5346.
[62] S. J. Aton, C. S. Colwell, A. J. Harmar, J. Waschek, E. D. Herzog, Vasoactive intestinal polypeptide mediates circadian rhythmicity and synchrony in mammalian clock neurons, Nat. Neurosci. 8 (4) (2005) 476–483.
[63] S. J. Aton, J. E. Huettner, M. Straume, E. D. Herzog, Gaba and gi/o differentially control circadian rhythms and synchrony in clock neurons, Proc. Natl. Acad. Sci. U. S. A. 103 (50) (2006) 19188–19193.
[64] J. A. Evans, T. L. Leise, O. Castanon-Cervantes, A. J. Davidson, Dynamic interactions mediated by nonredundant signaling mechanisms couple circadian clock neurons, Neuron 80 (4) (2013) 973–983.
[65] J. Myung, S. Hong, D. DeWoskin, E. De Schutter, D. B. Forger, T. Takumi, Gaba-mediated repulsive coupling between circadian clock neurons in the scn encodes seasonal time, Proc. Natl. Acad. Sci. 112 (29) (2015) E3920–E3929.
[66] H. Albus, M. J. Vansteensel, S. Michel, G. D. Block, J. H. Meijer, A gabaergic mechanism is necessary for coupling dissociable ventral and dorsal regional oscillators within the circadian clock, Curr. Biol. 15 (10) (2005) 886–893.
[67] D. DeWoskin, J. Myung, M. D. C. Belle, H. D. Piggins, T. Takumi, D. B. Forger, Distinct roles for gaba across multiple timescales in mammalian circadian timekeeping, Proc. Natl. Acad. Sci. (2015) 201420753.
[68] J. H. Abel, K. Meeker, D. Granados-Fuentes, P. C. St. John, T. J. Wang, B. B. Bales, F. J. Doyle III, E. D. Herzog, L. R. Petzold, Functional network inference of the suprachiasmatic nucleus, Proc. Natl. Acad. Sci. (2016) 201521178.
[69] J. A. Evans, T.-C. Suen, B. L. Callif, A. S. Mitchell, O. Castanon-Cervantes, K. M. Baker, I. Kloehn, K. Baba, B. J. Teubner, J. C. Ehlen, K. N. Paul, T. J. Bartness, G. Tosini, T. Leise, A. J. Davidson, Shell neurons of the master circadian clock coordinate the phase of tissue clocks throughout the brain and body, BMC Biol. 13 (1) (2015) 43.
[70] J. Bass, J. S. Takahashi, Circadian integration of metabolism and energetics, Science 330 (6009) (2010) 1349–1354.
[71] F. Damiola, Restricted feeding uncouples circadian oscillators in peripheral tissues from the central pacemaker in the suprachiasmatic nucleus, Genes Dev. 14 (23) (2000) 2950–2961.
[72] J. K. Kim, D. B. Forger, A mechanism for robust circadian timekeeping via stoichiometric balance, Mol. Syst. Biol. 8 (1) (2012) 630.
[73] P. O. Westermark, D. K. Welsh, H. Okamura, H. Herzel, Quantification of circadian rhythms in single cells, PLoS Comput. Biol. 5 (11) (2009) e1000580.
[74] H. Koeppl, M. Hafner, A. Ganguly, A. Mehrotra, Deterministic characterization of phase noise in biomolecular oscillators, Phys. Biol. 8 (5) (2011) 055008.
[75] R. J. Field, Oscillations in chemical systems. iv. limit cycle behavior in a model of a real chemical reaction, J. Chem. Phys. 60 (5) (1974) 1877.
[76] B. van der Pol, Lxxxviii. on relaxation-oscillations, London, Edinburgh, Dublin Philos. Mag. J. Sci. 2 (11) (1926) 978–992.
[77] J. Huang, D. L. Turcotte, Are earthquakes an example of deterministic chaos?, Geophys. Res. Lett. 17 (3) (1990) 223–226.
[78] P. C. St. John, S. R. Taylor, J. H. Abel, F. J. Doyle III, Amplitude metrics for cellular circadian bioluminescence reporters, Biophys. J. 107 (11) (2014) 2712–2722.
[79] C. S. Pittendrigh, S. Daan, A functional analysis of circadian pacemakers in noctural rodents: I. the stability and lability of circadian frequency, J. Comp. Physiol. A 106 (1976) 223–252.
[80] M. H. Vitaterna, C. H. Ko, A.-M. Chang, E. D. Buhr, E. M. Fruechte, A. Schook, M. P. Antoch, F. W. Turek, J. S. Takahashi, The mouse clock mutation reduces circadian pacemaker amplitude and enhances efficacy of resetting stimuli and phase-response curve amplitude, Proc. Natl. Acad. Sci. U. S. A. 103 (24) (2006) 9327–9332.
[81] M. Comas, D. G. M. Beersma, K. Spoelstra, S. Daan, Phase and period responses of the circadian system of mice (mus musculus) to light stimuli of different duration, J. Biol. Rhythms 21 (5) (2006) 362–372.
[82] S. R. Pulivarthy, N. Tanaka, D. K. Welsh, L. De Haro, I. M. Verma, S. Panda, Reciprocity between phase shifts and amplitude changes in the mammalian circadian clock, Proc. Natl. Acad. Sci. 104 (51) (2007) 20356–20361.
[83] H. Ukai, T. J. Kobayashi, M. Nagano, K.-H. Masumoto, M. Sujino, T. Kondo, K. Yagita, Y. Shigeyoshi, H. R. Ueda, Melanopsin-dependent photo-perturbation reveals desynchronization underlying the singularity of mammalian circadian clocks singularity behaviour in circadian clocks, Nat. Cell Biol. 9 (11) (2007) 1327–1334.
[84] B. Novák, J. J. Tyson, Design principles of biochemical oscillators, Nat. Rev. Mol. Cell Biol. 9 (12) (2008) 981–991.
[85] H. Rabitz, M. Kramer, D. Dacol, Sensitivity analysis in chemical kinetics, Annu. Rev. Phys. Chem. 34 (1) (1983) 419–461.
[86] M. A. Kramer, H. Rabitz, J. M. Calo, Sensitivity analysis of osciallatory systems, Appl. Math. Model. 8 (1984) 328–340.
[87] Y. Kuramoto, Chemical oscillations, waves, and turbulence, Springer, 1984.
[88] D. Gonze, J. Halloy, A. Goldbeter, Robustness of circadian rhythms with respect to molecular noise, Proc. Natl. Acad. Sci. 99 (2) (2002) 673–678.
[89] J. N. Teramae, D. Tanaka, Robustness of the noise-induced phase synchronization in a general class of limit cycle oscillators, Phys. Rev. Lett. 93 (20) (2004) 1–4.
[90] L. Glass, Synchronization and rhythmic processes in physiology, Nature 410 (6825) (2001) 277–284.
[91] O. Slaby, S. Sager, O. S. Shaik, U. Kummer, D. Lebiedz, Optimal control of self-organized dynamics in cellular signal transduction, Math. Comput. Model. Dyn. Syst. 13 (5) (2007) 487–502.
[92] N. Bagheri, J. Stelling, F. Doyle III, Circadian phase entrainmentvia nonlinear model predictive control, Int. J. Robust Nonlinear Control 17 (17) (2007) 1555–1571.
[93] O. Shaik, S. Sager, O. Slaby, D. Lebiedz, Phase tracking and restoration of circadian rhythms by model-based optimal control, IET Syst. Biol. 2 (1) (2008) 16–23.
[94] E. B. Klerman, H. B. Gershengorn, J. F. Duffy, R. E. Kronauer, Comparisons of the variability of three markers of the human circadian pacemaker, J. Biol. Rhythms 17 (2) (2002) 181–193.
[95] V. Kolodyazhniy, J. Späti, S. Frey, T. Götz, A. Wirz-Justice, K. Kräuchi, C. Cajochen, F. H. Wilhelm, Estimation of human circadian phase via a multi-channel ambulatory monitoring system and a multiple regression model, J. Biol. Rhythms 26 (1) (2011) 55–67.
[96] O. J. Walch, A. Cochran, D. B. Forger, A global quantification of "normal" sleep schedules using smartphone data, Sci. Adv. 2 (5) (2016) e1501705–e1501705.
[97] T. Hirota, J. W. Lee, W. G. Lewis, E. E. Zhang, G. Breton, X. Liu,

M. Garcia, E. C. Peters, J.-P. Etchegaray, D. Traver, P. G. Schultz, S. A. Kay, High-throughput chemical screen identifies a novel potent modulator of cellular circadian rhythms and reveals ckiα as a clock regulatory kinase, PLoS Biol. 8 (12) (2010) e1000559.

[98] P. C. St. John, T. Hirota, S. A. Kay, F. J. Doyle III, Spatiotemporal separation of per and cry posttranslational regulation in the mammalian circadian clock, Proc. Natl. Acad. Sci. U. S. A. 111 (5) (2014) 2040–2045.

[99] S. An, R. Harang, K. Meeker, D. Granados-Fuentes, C. A. Tsai, C. Mazuski, J. Kim, F. J. Doyle III, L. R. Petzold, E. D. Herzog, A neuropeptide speeds circadian entrainment by reducing intercellular synchrony, Proc. Natl. Acad. Sci. U. S. A. 110 (46) (2013) E4355–E4361.

[100] N. J. Kingsbury, S. R. Taylor, M. A. Henson, Inhibitory and excitatory networks balance cell coupling in the suprachiasmatic nucleus: A modeling approach, J. Theor. Biol. 397 (2016) 135–144.

[101] J. Andersson, J. Akesson, M. Diehl, Recent Advances in Algorithmic Differentiation, Vol. 87, Springer Berlin Heidelberg, 2012.

[102] L. Petzold, A. Hindmarsh, Lsoda (livermore solver of ordinary differential equations), Comput. Math. Res. Div. Lawrence Livermore Natl. Lab. Livermore, CA.